Globular Porous Nanoparticle Tin(IV) Phenylphosphonates and Mixed Methyl Phenylphosphonates

Jin Huang, Ayyappan Subbiah, David Pyle,[#] Adam Rowland,[#] Brentley Smith,[#] and Abraham Clearfield*

Department of Chemistry, Texas A&M University, P. O. Box 30012, College Station, Texas 77842-3012

Received June 7, 2006. Revised Manuscript Received August 21, 2006

Hydrothermal synthesis of $Sn(O_3PC_6H_5)_2$ yields globular aggregates of nanoparticles that are layered. The particle size depends upon the time and temperature of hydrothermal treatment but may be as small as 20 nm in the lateral directions and three or four layers thick. Because of their small size, the particles form globules within which the particles form "house of cards" type pores. Surface areas as high as 300 m^2/g are common with pores in the micropore range. Tin(IV) methylphosphonate is also layered, but the particles tend to aggregate into rosettes. Mixed derivatives of the type $Sn(O_3PC_6H_5)_x(O_3PCH_3)_{2-x}$, where $x > 0.5$, also form globules, with higher surface areas than the tin phenylphosphonates. The formation of these spherical aggregates appears to be general for tin(IV) phosphonates as a result of a lack of particle growth.

1. Introduction

The study of inorganic −organic hybrid materials is a field of chemistry that gives rise to materials with unique and promising properties. Among the many types of hybrids that have been reported, one area that has been significantly explored is that of metal phosphonates.[1] As thin films constituted from layer-by-layer assembly,[2] they have been designed to have nonlinear optical properties[3,4] and photochemical behavior,[5] to act as sensors,[6] and to enhance electron-transfer reactions.[7] A broad array of porous phosphonates has also been prepared.[8] Some are tubular and based on copper[9] and aluminum.[10] Other types result from pillared layered structures in which the pillars may be spaced to provide porosity.[11,12] Another strategy involves the use of diphosphonate blocks that can connect both phosphonic acid groups to metal atoms on the same layer while also cross-linking adjacent layers.[13] This technique spreads the pillars further apart, creating porous regions between the layers.

Recently, it was reported that porous tin(IV) phenylphosphonate could be prepared by a nonhydrolytic sol−gel route or by the use of surfactants.[14] The composition was reported as $Sn(O_3PC_6H_5)_2 \cdot H_2O$. Using sodium dodecylsulfate (SDS) as the template, researchers found the product to be microporous; however, in the absence of SDS, the tin phosphonate was mesoporous with a broad distribution of pore sizes. These results were of interest to us because the analogous Zr compound is layered and nonmicroporous.[15] Our preliminary study[16] revealed that, indeed, porous compounds resulted from nonsurfactant or template-assisted synthesis. We used quite a broad range of phosphonic acid ligands in this earlier study, all of which resulted in porous products. The reason lies in the fact that the resulting particles

* Corresponding author. E-mail: clearfield@mail.chem.tamu.edu.
[#] Undergraduate student.

(1) Clearfield, A. In *Metal Phosphonate Chemistry in Progress in Inorganic Chemistry*; Karlin, K. D., Ed.; John Wiley: New York, 1998; pp 371−510.
(2) (a) Lee, H.; Kepley, L. J.; Mallouk, T. E.; Hong, H. G.; Ahkter, S. J. *J. Phys. Chem.* **1988**, *92*, 2597. (b) Lee, H.; Kepley, L. J.; Hong, H. G.; Mallouk, T. E. *J. Am. Chem. Soc.* **1988**, *110*, 618.
(3) Katz, H. E.; Scheller, G.; Putvinski, T. M.; Schilling, M. L.; Wilson, W. L.; Chidsey, C. E. D. *Science* **1991**, *254*, 1485.
(4) Katz, H. E.; Wilson, W. L.; Chidsey; Scheller, G. *J. Am. Chem. Soc.* **1994**, *116*, 6636.
(5) Vermeulen, L. A.; Thompson, M. E. *Chem. Mater.* **1994**, *6*, 77.
(6) (a). Brousseau, L. C.; Mallouk, T. E. *Anal. Chem.* **1997**, *69*, 679. (b). Brousseau, L. C.; Aurentz, D. J.; Benesi, A. J.; Mallouk, T. E. *Anal. Chem.* **1997**, *69*, 688.
(7) Hoertz, P. G.; Mallouk, T. E. *Inorg. Chem.* **2005**, *44*, 6828.
(8) (a) Poojary, D. M.; Grohol, D.; Clearfield, A. *Angew. Chem., Int. Ed.* **1995**, *34*. 1508. (b) Poojary, D. M.; Cabeza, A.; Aranda, A. G.; Bruque, S.; Clearfield, A. *Inorg. Chem.* **1996**, *35*, 1468.
(9) Bideau, J. L.; Palvadeau, P.; Bujoli, B. *Inorg. Chem.* **1994**, *33*, 4885.
(10) (a) Maeda, K.; Kiyozumi, Y.; Mizukami, F. *Angew. Chem., Int. Ed.* **1994**, *33*, 2335. (b) Maeda, K.; Akimoto, J.; Kiyozumi, Y.; Mizukami, F. *J. Chem. Soc., Chem. Commun.* **1995**, 1033. (c) Maeda, K.; Akimoto, J.; Kiyozumi, Y.; Mizukami, F., *Angew. Chem., Int. Ed.* **1995**, *34*, 1199. (d) Haskouri, J. E.; Guillem, C.; Latorre, J. Beltran, A.; Beltran, D.; Amoros, P. *Chem. Mater.* **2004**, *16*, 4359.
(11) (a) Alberti, G.; Costantino, U.; Marmottini, F.; Vivani, R.; Zappelli, P. *Angew. Chem., Int. Ed.* **1993**, *32*, 1357. (b) Alberti, G.; Marmottini, F.; Murcia, M.; Vivani, R.; Zappelli, P. *Angew. Chem., Int. Ed.* **1994**, *33*, 1594.
(12) (a) Byrd, H.; Reis, K. P.; Poojary, D. M.; Clearfield, A.; Thompson, M. E. *Chem. Mater.* **1996**, *8*, 2239. (b) Clearfield, A. *Chem. Mater.* **1998**, *10*, 2801. (c) Clearfield, A.; Wang, Z.; Bellinghausen, P. *J. Solid State Chem.* **2002**, *167*, 376. (d) Clearfield, A.; Wang, Z. *J. Chem. Soc., Dalton Trans.* **2002**, 2937. (e) Wang, Z.; Heising, J.; Clearfield, A. *J. Am. Chem. Soc.* **2003**, *125*, 10375. (f) Gómez-Alcántara, M. M.; Cabeza, A.; Moreno-Real, L.; Aranda, M. A. G.; Clearfield, A. *Microporous Mesoporous Mater.* **2006**, *88*, 293.
(13) (a) Penicaud, V.; Massiot, D.; Gelbard, G.; Odobel, F.; Bujoli, B. *J. Mol. Struct.* **1998**, *469*, 31. (b) Vivani, R.; Costantino, U.; Nocchetti, M. *J. Mater. Chem.* **2002**, *12*, 3254.
(14) (a) Mal, N. K.; Fujiwara, M.; Yamada, Y.; Matsukata, M. *Ceram. Lett.* **2003**, *111*, 219. (b) Mal, N. K.; Fujiwara, M.; Yamada, Y.; Matsukata, M. *Chem. Lett.* **2003**, *32*, 292. (c) Mal, N. K.; Fujiwara, M.; Yamada, Y.; Matsukata, M. *Chem. Commun.* **2005**, 5199.
(15) (a) Alberti, G.; Costantino, U.; Allulli, S.; Tomassini, N. *J. Inorg. Nucl. Chem.* **1978**, *40*, 1113. (b) Poojary, D. M.; Hu, H.-L.; Campbell, F. L., III; Clearfield, A. *Acta Crystallogr., Sect. B* **1993**, *49*, 996.
(16) Subbiah, A.; Pyle, D.; Rowland, A.; Huang, J.; Narayanan, R. A.; Thiyagarajan, P.; Zón, J.; Clearfield, A. *J. Am. Chem. Soc.* **2005**, *127*, 10826.

10.1021/cm061333j CCC: $33.50
Published on Web 10/05/2006

were nanosized and aggregated into spheres with interparticle pores. In this paper, we describe the synthesis and characterization of the phenyl, methyl, and mixed phenyl−methyl derivatives.

2. Experimental Section

2.1. Materials. Commercially available starting reagents, tin(IV) chloride pentahydrate ($SnCl_4 \cdot 5H_2O$, 98%), methylphosphonic acid ($CH_3PO_3H_2$, 98%), and phenylphosphonic acid ($C_6H_5PO_3H_2$, 98%) were obtained from Aldrich and used without further purification. Hydrofluoric acid (HF, 48% solution) was obtained from EM Science and used as received. The Teflon-lined steel pressure vessels used in all the hydrothermal experiments were manufactured by the departmental mechanical shop of Texas A&M University, Department of Chemistry.

2.2. Synthesis. The following tin(IV) phosphonates were synthesized: tin(IV) phenylphosphonate, $Sn(O_3PC_6H_5)_2$, tin(IV) methylphosphonate, $Sn(O_3PCH_3)_2$, and phenyl−methyl mixed phosphonates, $Sn(O_3PC_6H_5)_x(O_3PCH_3)_{2-x}$. In all cases, the reaction reagents were first mixed at room temperature, and the mixtures were then refluxed or heated hydrothermally.

Typical hydrothermal preparations are given below. In an example of the preparation of $Sn(O_3PC_6H_5)_2$, 1.0518 g (3 mmol) of $SnCl_4 \cdot 5H_2O$ was placed into a plastic beaker. DI water (10 mL) and 0.25 mL (7 mmol) of HF solution were then added. In a separate beaker, 0.9486 g (6 mmol) of $C_6H_5PO_3H_2$, 5 mL of ethanol, and 5 mL of distilled deionized (DDI) water were mixed together and stirred. Once the ligand ceased to dissolve, the two solutions were combined, leading to the immediate formation of a white suspension/gel. The mixture was then sealed and heated at 140 °C for 3 days. The resulting white powder was filtered off and washed with ethanol and water. It was then dried at 60 °C overnight to yield about 1.23 g of solid (Sn-based yield of 96%). Reactions were also done without the addition of HF.

The synthesis of $Sn(O_3PCH_3)_2$ follows the same general synthesis patterns outlined above except for substituting 0. 5761 g (6 mmol) of $CH_3PO_3H_2$ for the $C_6H_5PO_3H_2$. In the synthesis of $Sn(O_3PC_6H_5)(O_3PCH_3)$, 0.4743 g (3 mmol) of $C_6H_5PO_3H_2$ and 0.2880 g (3 mmol) of $CH_3PO_3H_2$ were mixed in an ethanol/H_2O solution and later combined with $SnCl_4 \cdot 5H_2O$ solution (3 mmol, in DDI water and HF). Approximately 1.02 g of a white powder product was usually obtained in this case. The calculated Sn-based yield is approximately 92%, slightly lower than that of $Sn(O_3PC_6H_5)_2$. Variation of temperature, time, and ligand ratio in the synthesis were also carried out. Further synthesis experiments on the mixed-component phosphonate were carried out by varying the ratio of two phosphonic acids and the amount of HF used in the system. In general, three starting $C_6H_5PO_3H_2$:$CH_3PO_3H_2$ molar ratios were chosen in the studies. They were 3:1, 1:1, and 1:3, and a second series of ratios of 2:1, 1:1, and 1:2.

All products collected were washed repeatedly with water and ethanol before any further characterization. Silver nitrate test was employed to ensure no presence of Cl^- in the final products. Electron microprobe measurements on selected samples showed a negligible presence of Cl^-.

2.3. Characterization. Powder X-ray diffraction patterns were recorded on both a Rigaku computer automated diffractometer (rotating anode, Cu Kα radiation, operating at 40 kV and 40−150 mA) and a Bruker D8 Advance powder X-ray diffractometer (Cu Kα radiation; operating at 40 kV and 40 mA) that was fitted with a diffracted beam monochromator and a scintillation counter. Data were collected by the $\theta/2\theta$ mode in Bragg−Brentano geometry over the general 2θ ranges 3−70°, with a step size of 0.02° and a counting time of 1 s/step. Synchrotron X-ray diffraction data set was collected at the 1-BM beamline at the Advanced Photon Source (APS), Argonne National Laboratory (ANL), using a MAR-345 image plate with X-rays of ~20 keV energy ($\lambda = 0.619355$ Å). The wavelength value is obtained by running a LaB_6 standard using an analyzer crystal.

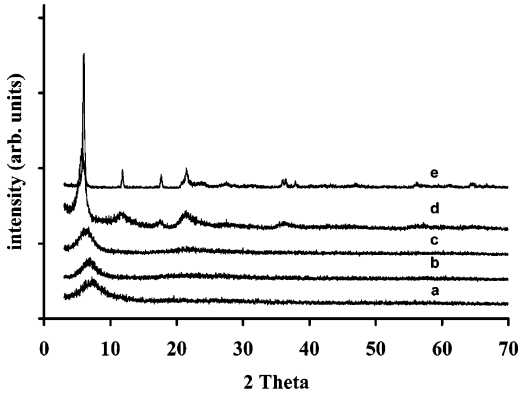

Figure 1. Powder XRD patterns of $Sn(O_3PC_6H_5)_2$. Samples were prepared by (a) room-temperature precipitation, (b) reflux for 1 h, (c) reflux for 12 h, (d) hydrothermal treatment at 140 °C for 3 days, (e) hydrothermal treatment at 220 °C for 30 days.

Scanning electron microscope (SEM) images were obtained with a Zeiss 1530 VP FE-SEM located in the Texas A&M University Electron Microscopy Center.

N_2 gas adsorption−desorption isotherms were performed on a Quantachrome Autosorb 6 instrument at 77 K. Prior to the measurements, the samples were generally heated overnight at 250 °C (on the basis of their TGA results). The resulting samples were then degassed at 225 °C for 18 h. Specific surface areas were determined by the multipoint BET method. The t-plot was used to calculate the microporous portion. Pore size distributions were plotted by the MP method. Thermogravimetric analyses (TGA) were performed on a TA Instruments TGA Q-500 at a heating rate of 10 °C/min under air.

All NMR spectra were acquired on a Bruker Avance Ultra-Shield 400 solid-state spectrometer for ^{119}Sn, ^{31}P, ^{13}C, and ^{19}F nuclei. Bruker probes equipped with 2.5−7 mm rotors were used. ^{119}Sn, ^{31}P, ^{13}C, and ^{19}F MAS (magic angle spinning) NMR spectra were recorded with various spinning rates; using cross-polarization sequences and recycle delays of 1−20 s. SnO_2 was used as an external reference for ^{119}Sn chemical shifts, $CFCl_3$, and $(NH_4)H_2PO_4$ as an external reference for ^{13}C, ^{19}F, and ^{31}P, chemical shifts, respectively.

FTIR spectra were measured on a Nicolet Nexus 470 FTIR spectrometer under nitrogen in KBr pellets. Elemental analyses (EA) were performed by Robertson Microlit. All proposed formulas were determined by considering EA, electron microprobe TGA, and solid-state NMR results.

3. Results and Discussion

3.1. $Sn(O_3PC_6H_5)_2$. The powder X-ray diffraction pattern of $Sn(O_3PC_6H_5)_2$, made by a typical hydrothermal method, is shown as pattern d in Figure 1. Generally, as-synthesized $Sn(O_3PC_6H_5)_2$ shows a poor degree of crystallinity, but details some structural features. The first feature is a large peak around 15 Å as the 001 reflection, and also the 002 reflection at about 7.5 Å. This is very similar to the powder patterns of the analogous Zr(IV) phenylphosphonate layered materials, identifying that the large peak may represent the interlayer spacing. There are other broad peaks that occur at

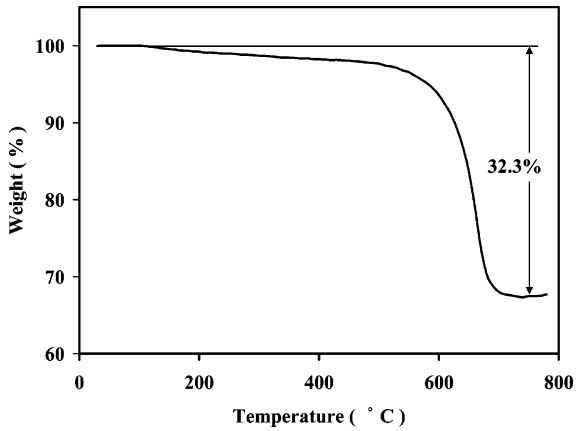

Figure 2. TG curve of $Sn(O_3PC_6H_5)_2$, showing a single-step weight loss of 32.3% of initial weight (calcd weight loss: 32.1%). The sample was prepared by hydrothermal treatment at 220 °C for 30 days without the presence of HF.

higher-angle regions, but the lack of structural data precludes conclusions as to what they indicate. An effort was made to improve sample crystallinity by longer heating at a higher temperature (220 °C) (Figure 1, pattern e) that is an order of magnitude better. However, it shows the effects of preferred orientation and is still insufficiently developed for structure solution. We note that only a single peak appears for samples prepared by the reflux method (Figure 1a−c).

Thermogravimetric analysis always showed only one significant mass loss (Figure 2). A long burn from 300 to 700 °C left only about 67% of the initial mass. Calculations indicate that $Sn(O_3PC_6H_5)_2$ burning to form SnP_2O_7 would leave 68% of the initial mass. This is within error when a small amount of solvent loss is considered. The residue was confirmed by PXRD to be SnP_2O_7.

Figure 3 shows MAS solid-state NMR spectra of the $Sn(O_3PC_6H_5)_2$ compound. The ^{119}Sn spectrum shows a single chemical shift of −821.5 ppm, suggesting the presence of eight-coordinated Sn(IV). This is concluded by comparing the value to that of six-coordinated Sn(IV) in SnO_2 at −600 ppm and those of several other eight-coordinated Sn(IV) compounds with chemical shifts around −800 ppm.[17] This dictates that the tin(IV) phenylphosphonate layers are considerably different from their zirconium analogue. The chemical shifts of ^{13}C are all in the phenyl ring region, and a single ^{31}P shift just confirms the proposed general formula of $Sn(O_3PC_6H_5)_2$. The shift of +4 for phosphorus compares to that of $Zr(O_3PC_6H_5)_2$ at −5.1 ppm.

Most tin phosphonates were prepared by the hydrothermal method.[16] The synthesis followed the general pattern outlined in the experimental section and was repeated a large number of times with a number of variations. These included the reaction temperature, heating duration time, and amount of HF and solvent. A few low-temperature experiments and their results are also included for comparison purposes. The quality of a synthetic method was mostly judged by examining total surface area, microporosity, and morphology of the as-synthesized samples. One of our objectives was to correlate synthetic conditions with the resulting product porosity to determine the optimum condition for preparing highly microporous materials of uniform pore dimensions.

Unlike Zr(IV) phenylphosphonates, which can be readily obtained by reacting $ZrOCl_2 \cdot 8H_2O$ with phenylphosphonic acid by low-temperature reflux or hydrothermal treatments, stoichiometric tin(IV) phenylphosphonate is incompletely formed at temperatures below 140 °C. Without the addition of HF, in which the starting reagents were simply mixed and stirred at room temperature for 6 h, a white amorphous product was obtained. Refluxing the same mixture for certain lengths of time gave similar poorly crystalline products (see Figure 1a−c). The incompleteness of the reaction is shown

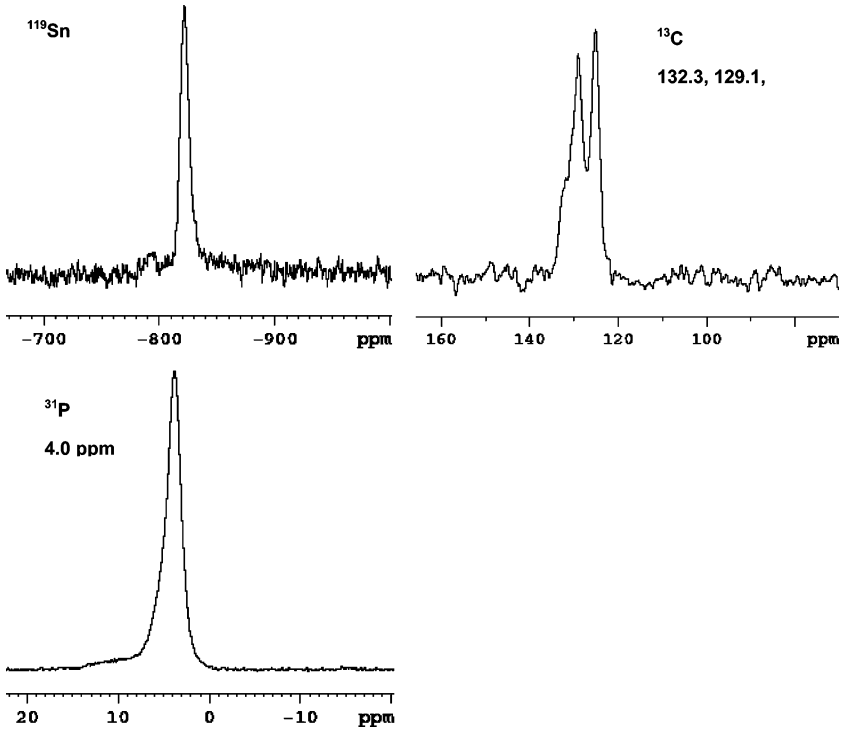

Figure 3. MAS solid-state NMR spectra of $Sn(O_3PC_6H_5)_2$. Chemical shifts of ^{119}Sn (top left), ^{13}C (top right), and ^{31}P (bottom) are as indicated.

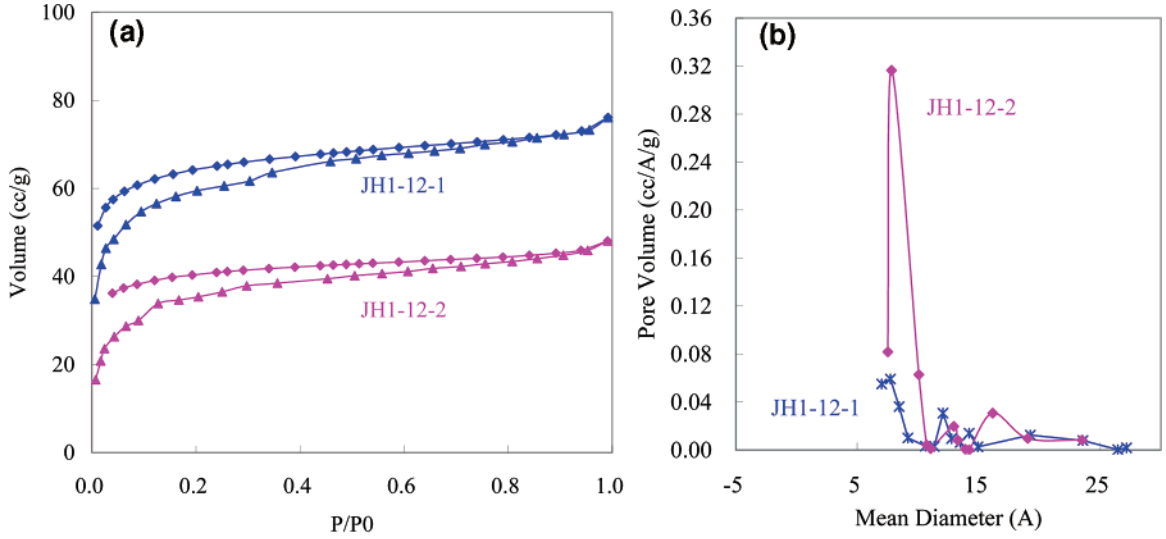

Figure 4. N_2 sorption−desorption isotherms of low-temperature $Sn(O_3PC_6H_5)_2$: (a) (▲) adsorption and (◆) desorption; (b) pore size distributions based on the isotherms.

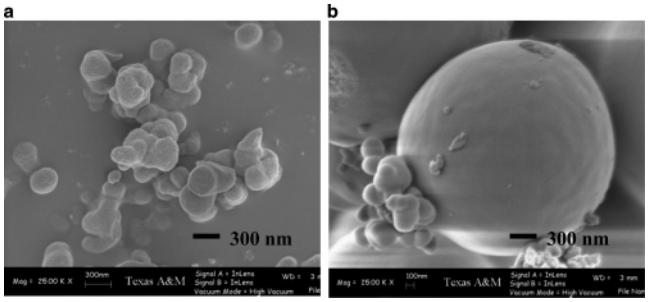

Figure 5. SEM micrographs of low-temperature $Sn(O_3PC_6H_5)_2$. (a) JH1-7-5, room temperature mixed for 6 h; (b) JH1-12-1; refluxed for 1 h. Some of the spheres have grown larger in the refluxed samples.

by the retention of Cl^-, H_2O, and F^- by the samples prepared below 140 °C for short periods of time. In the case of chloride retention, extensive washing removes the Cl^-. However, this removal may involve OH^- substitution for Cl^- bonded to Sn. When HF is added as a solublizing agent, NMR spectra contain no reasonable resonances, indicating bonding of F to tin. The conditions of preparation of the low-temperature preparations and the surface areas of the products are collected in Table 1. Although the products exhibited high surface areas and a microporous character, the N_2 sorption−desorption isotherms did not close (Figure 4), probably because of the incompleteness of the reaction. In our previous report,[16] it was shown that the hydrothermally prepared tin phosphonates form spherical aggregates. Therefore, it was of interest to see if the refluxed samples behaved similarly. Indeed, they do, as shown in Figure 5. In Figure 5A, where no refluxing was administered and the ingredients were merely stirred for 6 h, very small (100−300 nm) poorly formed spherical aggregates are evident. After refluxing for 6 h, some well-formed micrometer-sized spheres formed, along with the very small ones. The 12 h refluxed sample showed a much higher percentage of the large spheres. As we shall see in what follows, the porosity is of the interparticle type; this is not evident in the smooth surfaces of the spheres. In contrast, hydrothermal preparations at higher temperature give more-crystalline products. This can be seen by comparing patterns d and e in Figure 1 with the others. The former pattern was collected on a sample hydrothermally prepared at 140 °C, whereas the latter was recorded on a sample similarly prepared at 220 °C. The corresponding SEM micrographs (Figure 6) show that all of the globules are micrometer sized. However, micrographs on the sample heated at higher temperature showed detailed information on the aggregation of individual crystallites. As their isotherms (Figure 7) are compared, some interesting trends can be seen. The spheres in the 180 °C sample are smaller, but the individual particles are much bigger than those prepared at 140 °C in both length and thickness (∼30−40 nm long and 10−15 nm thick). The particle size difference is reflected in the N_2 adsorption−desorption isotherms in Figure 7. The sample prepared at 140 °C gave a slightly modified Type I isotherm. The surface area was 298 m^2/g, of which 290 m^2/g arises from micropores. In fact, the pore size distribution indicates the major portion of the pores is in the 10−20 Å range. In contrast, the isotherm for the 180 °C sample is a Type IV with a large hysteresis, indicative of a distribution of mesopores. In fact, only 57 m^2/g of the total surface area (229 m^2/g) is due to micropores. The decrease in the size of the spheres may be directly attributed to the larger particle size. As the particle size increases, the strength of the surface forces decreases, decreasing the ability of particle aggregation. Furthermore, the larger the particle size, the larger the pores created by a house of cards particle arrangement. Larger particles also would result in larger pores, as is observed.

The time of hydrothermal treatment has the same general effect as increasing the temperature. Identical mixes of Sn,

Table 1. Conditions of Preparation and Surface Areas of the Refluxed Samples of $Sn(O_3PC_6H_5)_2$.

sample	molar ratio Sn:PhP:HF	H_2O/EtOH (mL)	*T*/time (h)	total area/micropore area (m^2/g)
JH1-7-5	6:12:0	30/10	RT/6	196/182
JH1-12-1	6:12:0	30/10	reflux/1	221/210
JH1-12-2	6:12:0	30/10	reflux/12	132/123

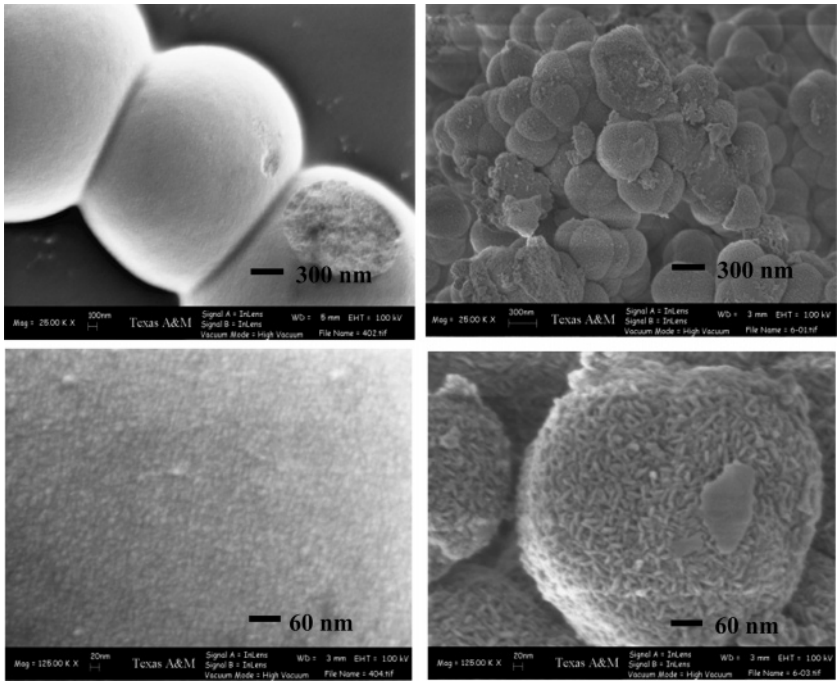

Figure 6. SEM micrographs of $Sn(O_3PC_6H_5)_2$ samples. Left: JH1-2-1 prepared at 140 °C for 3days; right: JH1-3-2 prepared at 180 °C for 3 days. Note that the globules have gotten smaller, but upon higher magnification, the individual particles are evident.

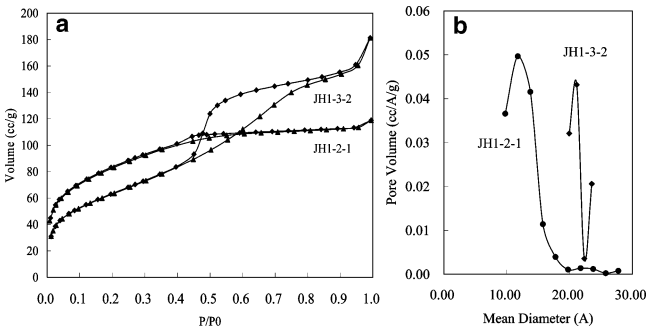

Figure 7. Isotherms of $Sn(O_3PC_6H_5)_2$. (a) JH1-2-1 prepared at 140 °C for 3 days and JH1-3-2 prepared at 180 °C for 3 days; (b) pore size distributions based on the isotherms.

HF, and phosphonic acid were treated hydrothermally at 140 °C for 1, 3, and 27 days. The sample heated for 1 day had a lower surface area (212 m^2/g) and a lesser proportion of micropores than the 3 day sample. The sample heated for 27 days contained larger individual particles and smaller sized spheres. Heating a sample at 220 °C for 30 days resulted in a nonmicroporous product with a modified Type IV isotherm with a high-pressure region indicative of the filling of macropores. The results are summarized in Table 2. The change in the isotherms is shown in Figure 8.

HF is generally used in the preparation of crystalline metal-(IV) phosphonates, as in the case of Zr(IV) compounds.[12] This is due to the formation of metal fluorocomplexes such as ZrF_6^{2-}, the slow decomposition of which introduces a controlled process under hydrothermal conditions, affording samples with a high degree of crystallinity. For the same reason, in some preparations of this study, HF was mixed with $SnCl_4 \cdot 5H_2O$ precursor solutions prior to further reaction, and corresponding comparison experiments with the absence of HF were also carried out. Surface area data (Table 3) indicate there is a significant increase in total surface area (by a minimum amount of 50 m^2/g) when a substantial amount of HF was added in the synthesis, accompanied by an increase in microporosity. When the HF:Sn ratio stayed at 7:3 (or 14:6), both total surface area and micropore area reached a maximum. Beyond the value of 7:3, a decrease in total surface area was observed without affecting microporosity. It is worth pointing out that very satisfactory surface area and microporosity can be achieved without using HF (as shown by data of JH1-3-1 in Table 3). ^{19}F solid-state NMR shows no presence of Sn−F bonding. A big broad peak in the NMR spectrum (not shown) results from the NMR rotor cap and sharp peaks, most probably from side bands coupled with a very small amount of an impurity.

In summary, the samples with high surface areas and regular micropores are obtained with Sn:PhP = 1:2, HF: n = 7:3, T = 140 °C, and heating time of 3 days.

3.2. $Sn(O_3PCH_3)_2$. Autoclaving a mixture of methylphosphonic acid and $SnCl_4$ at 140 °C for 3 days produced a poorly crystalline Sn methylphosphonate, $Sn(O_3PCH_3)_2$. The X-ray powder pattern (Figure 9, pattern a) shows some sharper and

Table 2. Conditions of Preparation and Surface Areas of Hydrothermally Prepared Samples of $Sn(O_3PC_6H_5)_2$.

sample	molar ratio Sn:PhP:HF	H_2O/EtOH (mL)	T/time (d)	total area/micropore area (m^2/g)
JH1-2-1	6:6:14	15/5	140/3	298/290
JH1-3-2	6:6:14	15/5	180/3	229/57
JH1-6-1	6:6:14	15/5	140 /1	212/97
JH1-2-1	6:6:14	15/5	140/3	298/290
JH1-6-2	6:6:14	15/5	140/27	209/192
JH1-10-2	3:6:0	15/5	220/20	149/0
JH1-9-3	3:6:0	15/5	220/30	57/0

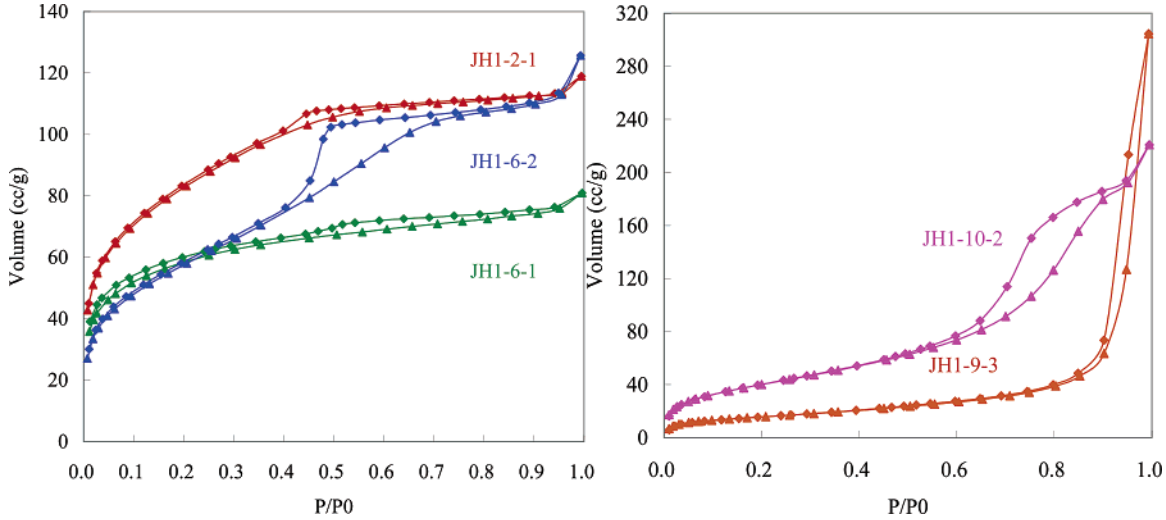

Figure 8. Time effect on hydrothermal preparations of $Sn(O_3PC_6H_5)_2$. N_2 adsorption−desorption isotherms for selected samples listed in Table 2. Note that samples heated at 220 °C for extended periods of time (right side) exhibited reduced surface areas and no micropores.

Table 3. Conditions of Preparation and Surface Areas of Hydrothermally Prepared Samples of $Sn(O_3PC_6H_5)_2$.

sample	molar ratio Sn: PhP:HF	H_2O/EtOH (mL)	*T*/time (h)	total area/micropore area (m^2/g)	pore size at curve max. (Å)
JH1-3-1	6: 6: 0	15/5	140/3	259/226	12.3
DP-4-1	6: 6: 9	15/5	140/3	307/300	14.7
ASI-20-4	6: 6: 14	15/5	140/3	327/317	11.8

more intense peaks than the sample of prepared phenylphosphonate under the same conditions, whose PXRD is given as pattern d in Figure 1. But broad peaks are also present, indicative of small, poorly formed crystallites. However, the problem displays the same features of layered structures, with the d_{001} spacing at 9.8 Å and the d_{002} at 4.9 Å, compared with 15.4 and 7.7 Å for $Sn(O_3PC_6H_5)_2$. Comparison of X-ray pattern e in Figure 1 with that of c in Figure 9 shows that a much more crystalline product is obtained for $Sn(O_3PCH_3)_2$ than for the phenyl analogue, as sample c was prepared at 180 °C for 30 days, whereas the phenyl derivative was prepared at 220 °C for the same length of time. The reason for the difference in sample crystallinity between Sn methylphosphonate and Sn phenylphosphonate is probably the greater solubility of the former compound in water than tin phenylphosphonate. The smaller d_{001} spacing is just a reflection of the size of methylphosphonic acid ligand. Highly crystalline tin methylphosphonate can be obtained by simultaneously increasing the temperature and heating time in the hydrothermal preparations. The X-ray powder pattern of a sample that was prepared by hydrothermal treatment at 180 °C for 15 days is shown in Figure 9b. Except for improved crystallinity, the pattern shows an effect of strong preferred orientation, which is commonly seen in the diffraction pattern of a layered structure. This effect is reinforced when a Bragg−Brentano laboratory diffractometer with flat-specimen stage is used to record the pattern.

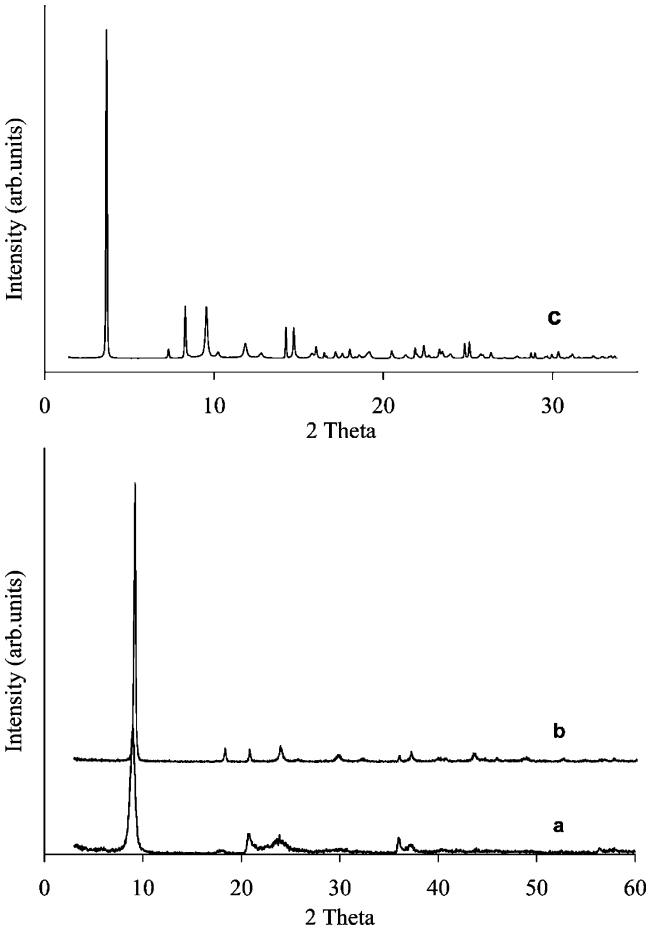

Figure 9. Powder XRD patterns of $Sn(O_3PCH_3)_2$. Sample **a** was prepared by hydrothermal method at 140 °C for 3 days; **b** was prepared at 180 °C for 15 days. Synchrotron data of $Sn(O_3PCH_3)_2$. Sample **c** was prepared at 180 °C for 30 days. The 2θ scale for **c** is 0−35°

The SEM examination of the $Sn(O_3PCH_3)_2$ samples prepared under mild hydrothermal conditions reveals a large rosette morphology (Figure 10, left). This is very different from that of $Sn(O_3PC_6H_5)_2$, which is dominated by small spheres of aggregated particles. Because the rosette can also

(17) (a) Kira, M.; Zhang, L. C.; Kabuto, C.; Sakurai, H. *Organometallics* **1998**, *17*, 887. (b) Tunstall, D. P.; Patou, S.; Liu, R. S.; Kao, Y. H. *Mater. Res. Bull.* **1999**, *34*, 1513. (c) Farcasiu, D.; Leu, R.; Ream, P. J. *J. Chem. Soc., Perkin Trans.* **2001**, *2*, 427. (d) Chaudhari, K.; Das, T. K.; Rajmohanan, P. R.; Lazar, K.; Sivasanker, S.; Chandwadkar, A. J. *J. Catal.* **1999**, *183*, 281.

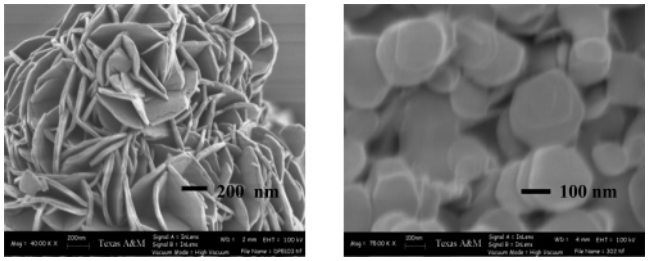

Figure 10. SEM micrographs of $Sn(O_3PCH_3)_2$. (a) ASI-21-4, as synthesized at 140 °C for 3 days; (b) LQ-1-09, synthesized at 180 °C for 30 days.

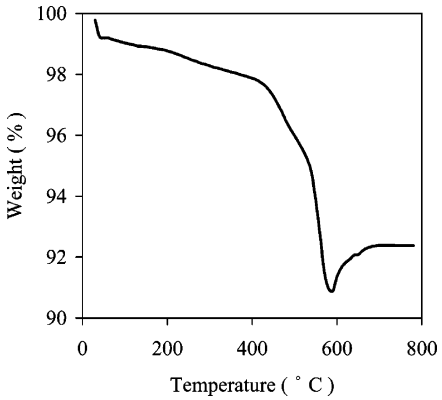

Figure 11. Typical TG curve of $Sn(O_3PCH_3)_2$, showing a single-step weight loss of ~6% of initial weight (calcd weight loss: 4.6%).

be considered as being layered particles clustered together, it is of interest to know what shape the individual particle can be. The micrograph (Figure 10, right) on the sample prepared at 180 °C for 30 days clearly shows that the rosette has already broken into thin platelets. The dimension of the plate averages at about 200 nm in diameter and 10 nm in thickness.

Synchrotron X-ray diffraction data on a highly crystalline tin methylphosphonate sample are shown in Figure 9c. Powder pattern indexing by different programs results in a small monoclinic cell: $a = 9.827(2)$ Å, $b = 4.992(1)$ Å, $c = 4.327(1)$ Å, $\beta = 98.25(4)°$. However, further structure solution attempts by using either direct methods or the Monte Carlo method brought no unique structure model. The problem preventing the structure solution is that these Sn phosphonates are nanoparticles. As indicated in the above SEM micrographs, even in the highly crystalline sample, the shortest dimensions of the nanodiscs are less than 10−20 nm, meaning that, on average, there are no more than 10 available layers for Bragg diffraction. Therefore, strain near the surface of the particles in one particular direction has to be accounted for, with some of the peaks being much broader, whereas others are not. Additional work is underway to prepare larger crystals of $Sn(O_3PCH_3)_2$ in order to obtain a structure solution.

Thermal analysis of $Sn(O_3PCH_3)_2$ gives a weight loss of ~6%, which is a little bit higher than the calculated 4.6% because of loss of surface water and solvent (Figure 11). The final weight loss is 7.6%, of which approximately 2% is water and perhaps trapped Cl^- as HCl. The curve dips lower than the required amount for the methylphosphonate at about 600 °C. This increased loss may result from preliminary formation of $Sn(PO_3)_2$, where the Sn(IV) is reduced to Sn(II) and then gains oxygen to form the pyrophosphate. The residue was identified as SnP_2O_7 by PXRD. The N_2 sorption−desorption isotherm is Type IV, indicative of all external surface (Figure 12).

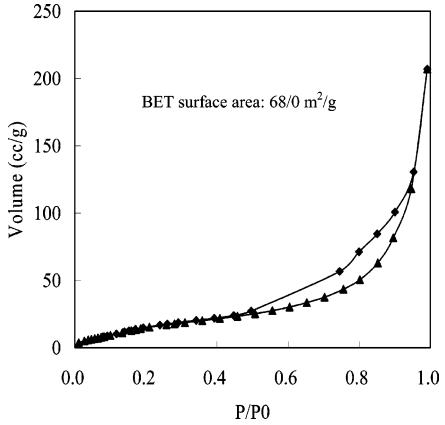

Figure 12. N_2 adsorption−desorption isotherm of $Sn(O_3PCH_3)_2$.

MAS solid-state NMR spectra of $Sn(O_3PCH_3)_2$ show character similar to that of $Sn(O_3PC_6H_5)_2$. A single chemical shift of −818.6 ppm in the ^{119}Sn spectrum again confirms that Sn(IV) is in an eight-coordinated position. The ^{31}P spectrum contains only a single peak at +13.3 ppm, which is in agreement with the proposed general formula of $Sn(O_3PCH_3)_2$. The ^{19}F NMR data is consistent with that of $Sn(O_3PC_6H_5)_2$.

Modification of a few hydrothermal synthetic parameters such as temperature and time does not change the porosity of $Sn(O_3PCH_3)_2$. All samples prepared under different conditions gave Type IV isotherms with a narrow span of total surface area from 48 to 68 m^2/g and micropore contribution of 0. Figure 12 shows the isotherm of a sample prepared under general hydrothermal condition. It is proper to conclude that the $Sn(O_3PCH_3)_2$ is nonmicroporous and the surface area is all external, that is, between individual plates.

3.3. $Sn(O_3PC_6H_5)_x(O_3PCH_3)_{2-x}$. Part of our research goal is to prepare porous solid materials with molecular architectures where porosity can potentially be tailored. One strategy for preparing such materials from layered metal phosphonates is to use a mixture of phosphonic acids in which one is a small molecule spacer, $R\text{-}PO_3H_2$ or $H_2PO_3\text{-}R\text{-}PO_3H_2$, where the pendent R groups are of different size. In this study, we have prepared a mixed-component tin(IV) phosphonate, $Sn(O_3PC_6H_5)_x(O_3PCH_3)_{2-x}$, by combining a mixture of phenylphosphonic acid and methylphosphonic acid with tin tetrachloride, as detailed in Table 4.

Figure 13a displays the powder X-ray diffraction patterns of $Sn(O_3PC_6H_5)_x(O_3PCH_3)_{2-x}$, with x varying discretely from 2 to 0, together with the TGA curves of the mixed derivatives. All the mixed-component samples were found to be poorly crystalline and retain characteristics of layered compounds. No phase separation of phases was observed as compared to the pattern of pure tin(IV) phenylphosphonate and tin(IV) methylphosphonate. This confirms that the phenyl and methyl phosphonate mixture are not bimodal, but that the two ligands are in fact interspersed throughout the structure. Furthermore, increasing methylphosphonic acid in the mixture decreases the d_{001} spacing value only when the amount of the spacer ligand exceeds that of the larger phenylphosphonic acid ligand.

Table 4. Conditions of Preparation, Surface Areas, and TGA Weight Losses of Hydrothermally Prepared Samples of $Sn(O_3PC_6H_5)_x(O_3PCH_3)_{2-x}$

sample	[Sn] (mmol)	molar ratio PhP:MeP (mmol)	[HF] (mmol)	surface areas total/micro (m^2/g)	d_{001} (Å)	TGA weight loss exp/calcd (%)
SnPhP	6	6:0	14	298/290	~15.4	31.92/32.03
a	6	4:2	14	321/307	~15.9	26.88/24.86
b	6	3:3	14	420/406	~15.2	22.60/20.65
c	6	2:4	14	323/262	~13.6	14.96/14.67
SnMeP	6	0:6	14	68/0	~9.87	6.00/4.59
d	3	4.5:1.5	7	365/350	~15.7	28.17/26.81
e	3	3:3	7	453/429	~15.1	22.50/20.65
f	3	1.5:4.5	7	384/341	~13.2	14.05/13.35

Table 5. Conditions of Preparation and Surface Areas of Hydrothermally Prepared Samples of $Sn(O_3PC_6H_5)_x(O_3PCH_3)_{2-x}$

sample	Sn	molar ratio PhP: MeP	HF	H_2O/EtOH (mL)	*T*/time (°C/day)	total/micropore area (m^2/g)
a	3	3:3		15/5	140/3	428/298
b	3	3:3	7	15/5	140/3	416/394
c	3	3:3	14	15/5	140/3	288/278
d	3	3:3	21	15/5	140/3	202/192

In the TG analyses of $Sn(O_3PC_6H_5)_x(O_3PCH_3)_{2-x}$, a general single gradual mass loss between 400 and 700 °C was observed for all the samples. The expected weight loss depended upon the ratio of the two ligands, and the weight loss observed was close to the predicted value (Figure 13b). Sample b showed a minor loss of mass (2−3%) below 100 °C, which is probably solvent retained by the pores. The calculated values were made on the assumption that the end product was SnP_2O_7.

Synthesis modifications of $Sn(O_3PC_6H_5)_x(O_3PCH_3)_{2-x}$ focused on varying the $C_6H_5PO_3H_2$:$CH_3PO_3H_2$ ratio and the amount of HF while holding other variables such as temperature and time constant at 140 °C/3 days. This is relying on the fact that layered Sn phenylphosphonates demonstrated satisfactory and controllable porosity under hydrothermal conditions. Introduction of the smaller methyl pendent group into the layered structures may create more internal space, thus leading to highly porous materials. Table 4 shows two groups of hydrothermal preparations and associated surface area results, with the only synthetic variable being the phenylphosphonic acid:methylphosphonic acid ratio. Samples for which the two ligands were present in equal amounts or the phenylphosphonic acid was present in greater amount (samples a, b, d, and e) exhibited Type I isotherms. The surface areas were large and the pores were largely in the micropore range. In contrast, samples c and f, for which the methylphosphonic acid was present in a greater amount, yielded essentially Type IV isotherms with high hysteresis effects and a greater spread of pore diameters. Clearly, the best molar ratio in terms of surface area obtained and microporosity was 1:1 $C_6H_5PO_3H_2$:$CH_3PO_3H_2$. In general, the mixed-component samples have higher surface area values than those of pure tin phenylphosphonates, so that adding a small methyl pendent group into a layered structure as a spacer is an effective way to create internal porosity and highly porous materials.

All the preparations mentioned above were done with the inclusion of HF. Although it is not clear what exact role the HF is playing, in these reactions, it was found to be indispensable in preparing microporous $Sn(O_3PC_6H_5)_x(O_3PCH_3)_{2-x}$. Table 5 and Figure 14 show how the amount of HF affects the microporosity of the mixed-component sample. The preparations were carried out with a 1:1 $C_6H_5PO_3H_2$:$CH_3PO_3H_2$ ratio and a fixed amount of tin tetrachloride under 140 °C for 3 days. As shown by surface area values and isotherms, the gradual increasing of HF:Sn decreased the sample surface area while increasing sample microporosity. For example, sample a was prepared without HF. It has the highest total surface area, 428 m^2/g, of which 298 m^2/g is from micropores, and a Type IV isotherm, indicative of the presence of considerable mesopores. When the HF:Sn ratio was increased from 7:3 to 14:3, and 21:3 in the starting mixture, the sample surface area dropped from 416/394 m^2/g to 288/278 m^2/g and 202/192 m^2/g, respectively. These

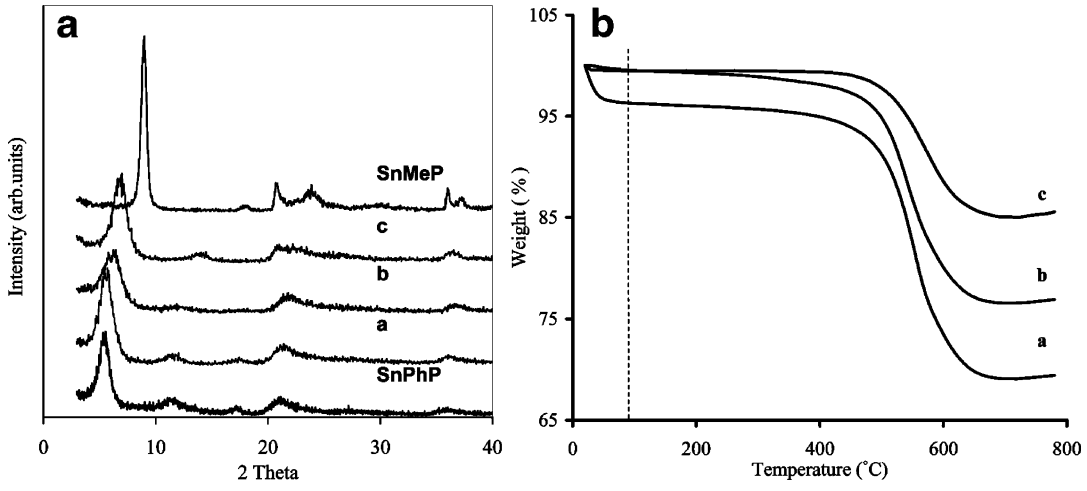

Figure 13. (a) Powder XRD patterns and (b) TG curves of $Sn(O_3PC_6H_5)_x(O_3PCH_3)_{2-x}$. Letters correspond to preparations listed in Table 4.

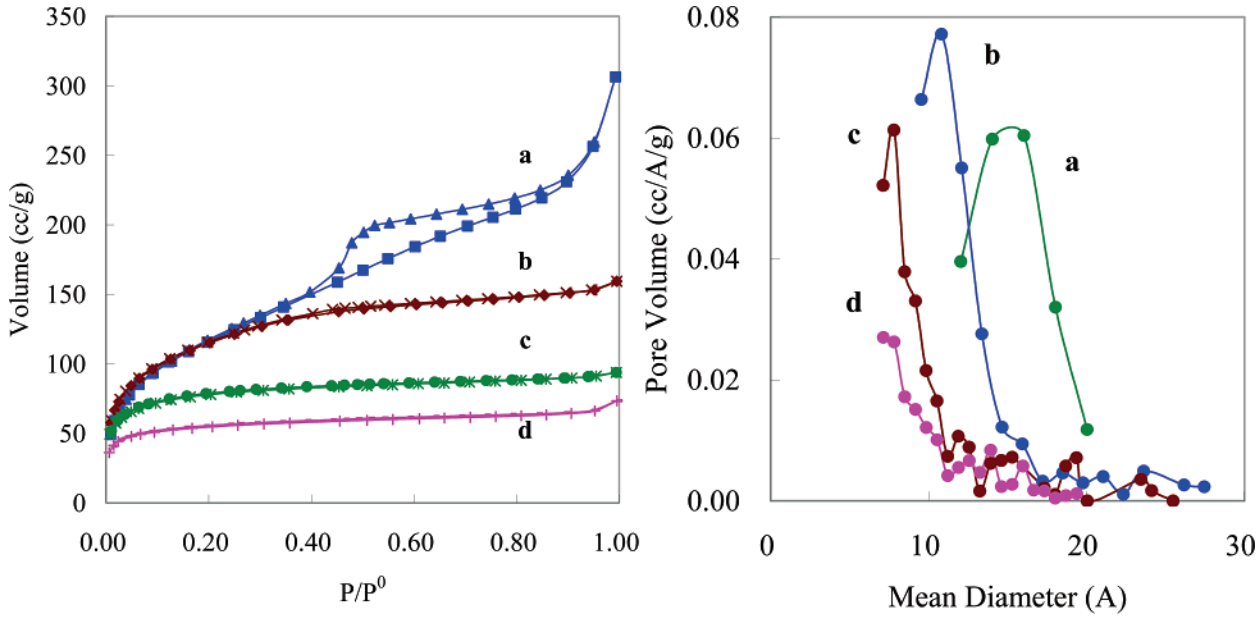

Figure 14. HF effect on preparations and isotherms of $Sn(O_3PC_6H_5)_x(O_3PCH_3)_{2-x}$. Letters correspond to preparations listed in Table 5.

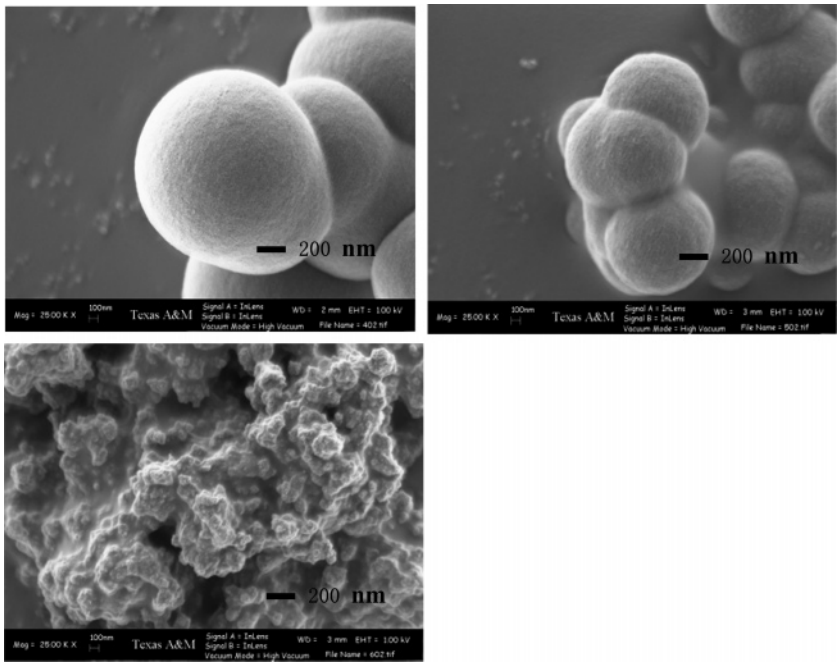

Figure 15. SEM micrographs of $Sn(O_3PC_6H_5)_x(O_3PCH_3)_{2-x}$. Top left, $x = 1.5$; top right, $x = 1$; bottom left, $x = 0.5$.

samples prepared with HF present all have Type I isotherms (Figure 14). The pore size distributions were calculated by the MP method for comparison. Mesopores are more likely to be developed without the presence of HF in the synthesis, as depicted by curve a (Figure 14) in the pore size distribution graphs. In summary, the HF effect found in the preparation of $Sn(O_3PC_6H_5)_x(O_3PCH_3)_{2-x}$ is in good agreement with that in $Sn(O_3PC_6H_5)_2$. The optimum synthetic conditions for highly microporous tin mixed phenyl−methyl phosphonates was, hydrothermal treatment of a mixture with Sn:HF:PhP:MeP ratios of 3:7:3:3 in water/ethanol solvent at 140 °C for 3 days.

SEM micrographs of $Sn(O_3PC_6H_5)_x(O_3PCH_3)_{2-x}$ are shown in Figure 15. The mixed-component sample having the most methylphosphonate groups no longer has a spherical morphology, showing the influence of the tin methylphosphonate rosettes. MAS solid-state NMR spectra of the sample with a 1:1 ratio show chemical shifts at (in ppm) ^{119}Sn, −817.1; ^{31}P, +15.4 and 4.0; ^{13}C, 132.9, 128.2, and 124.2; ^{19}F, −136 ppm. The results are consistent with the proposed general formula of $Sn(O_3PC_6H_5)(O_3PCH_3)$ and confirm the formation of a single phase compound instead of two separate phase products. A small amount of F^- is apparently bonded to Sn.

4. Conclusions

Recent chemistry of organic−inorganic hybrids has emphasized the synthesis of derivatives containing micro- and mesoporous structures. Many of these compounds were discovered by chance and many others by design. All of these compounds have a porosity that arises from creation of tunnels or cavities that are internal, which is a result of the

framework structure that encloses free space or space occupied by readily removable molecules.

The tin(IV) phosphonates reported here constitute a new way that porosity is developed. The individual particles are in the lower nanometer range when prepared under relatively mild conditions (140 °C, 3 days). Such particles are only a few layers thick as measured by SEM. Our hypothesis is that the nanoparticles aggregate into micrometer-sized spherical globules. The pores are then built up by the random arrangement of the particles. As the particles become larger through treatment at higher temperature and reaction times, the pore character changes also. Thus, the house of cards hypothesis appears to fit the present situation. Mixing a large and small ligand onto the same layer leads to additional porosity manifesting through internal pores.

The non-closing of the isotherms for the non-hydrothermally prepared samples is troublesome. We reran the samples at a larger equilibration time (10 min versus 3 min previously), but the isotherms did not close. However, they had reduced surface areas and slightly different shapes showing an aging effect. The interval between the first isotherms and the latter was 1 month. We observed high-resolution SEMs for two of the samples that revealed that the individual particles were in the size range 6−12 nm and their shape was close to spherical. This is in contrast to the samples prepared hydrothermally, which are flat platelets of layer size that form the house of cards pore. Thus the refluxed samples are amorphous metastable particles that are not stable under the conditions of measurement. We intend to further study the growth of these particles from conception to equilibrium status.

Acknowledgment. This study was supported by the National Science Foundation (NSF) through Grant DMR-0332453 and the Robert A. Welch Foundation Grant 0673A, for which grateful acknowledgment is made. The FE-SEM acquisition was supported by the NSF under Grant DBI-0116835. We also acknowledge the NSF (Grant CHE-0234931) for use of the solid-state 400 MHz NMR spectrometer. The synchrotron generated X-ray pattern was obtained at the Advanced Photon Source, Argonne National Laboratory, which is supported by the U.S. Department of Energy for which thanks is offered.

CM061333J